



A new numerical approach and visco-refined zigzag theory for blast analysis of auxetic honeycomb plates integrated by multiphase nanocomposite facesheets in hygrothermal environment

Mohammad Hadi Hajmohammad¹ · Amir Hossein Nouri¹ · Mohammad Sharif Zarei² · Reza Kolahchi³

Received: 23 August 2018 / Accepted: 15 October 2018 / Published online: 22 October 2018
© Springer-Verlag London Ltd., part of Springer Nature 2018

Abstract

The current work suggests a mathematical model for the dynamic response of sandwich plates subjected to a blast load using a numerical method. The sandwich structure is made from an auxetic honeycomb core layer integrated by multiphase nanocomposite facesheets. The facesheets are composed of polymer–carbon nanotube (CNT)–fiber where the equivalent material properties of the multiphase nanocomposite layers are obtained using fiber micromechanics and Halpin–Tsai equations in hierarchy. The top and bottom layers are subjected to magnetic field and the material properties of them are assumed temperature and moisture dependent. The Kelvin–Voigt model is employed to consider the viscoelastic properties of the structure. The sandwich structure is rested on a viscoelastic foundation which is modeled by orthotropic visco-Pasternak medium. Based on refined zigzag theory (RZT), energy method and Hamilton’s principle, the motion equations are derived. A new numerical method, namely differential cubature method (DCM) in conjunction with Newmark method is utilized for obtaining the dynamic deflection of the structure for different boundary conditions. The effects of various parameters such as blast load, viscoelastic foundation, structural damping, magnetic field, volume fraction of CNTs, temperature and moisture changes, geometrical parameters of honeycomb layer and sandwich plate are considered on the dynamic deflection of the structure. The results show that the magnetic field to the facesheets can be considered as effective parameters to control the dynamic deflection. In addition, hygrothermal condition leads to increase of 24% in the dynamic displacement of system.

Keywords Dynamic analysis · Blast load · Auxetic honeycomb core layer · Multiphase nanocomposite facesheets · Visco-refined zigzag theory

1 Introduction

The sandwich structures can be used in many industries such as automotive design and production, sport equipment fabrication, aeronautic, marine and oil industries due to high strength and low weight. One of the suitable candidates for the core layer is auxetic honeycomb material due to its excellent energy absorption capacity and high strength to weight

ratio. The facesheets of sandwich structure which are thinner than the core layer have many important roles in improving the strength of these structures. Polymer–CNT–fiber multiphase nanocomposite layers are a good choice for the layers of sandwich structures since adding a few weight percent of CNTs makes them much stiffer than steel while being three to five times lighter [1].

Dynamic analysis of sandwich plates with nanocomposite layers has been of intense interest among the researchers. The static response of an inhomogeneous fiber-reinforced viscoelastic sandwich plate was investigated by Allam et al. [2] using the first-order shear deformation theory. Large amplitude vibration problem of laminated composite spherical shell panel under combined temperature and moisture environment was analyzed by Mahapatra et al. [3]. Nguyen et al. [4] presented an isogeometric finite element formulation based on Bézier extraction of the non-uniform rational B-splines (NURBS) in combination with a generalized

✉ Reza Kolahchi
r.kolahchi@gmail.com

¹ Department of Mechanical Engineering, Imam Hossein University, Tehran, Iran

² Faculty of Engineering, Ayatollah Boroujerdi University, Boroujerd, Iran

³ Department of Civil Engineering, Meymeh Branch, Islamic Azad University, Meymeh, Iran

unconstrained higher order shear deformation theory (UHSDT) for laminated composite plates. The nonlinear free vibration behavior of laminated composite spherical shell panel under the elevated hygrothermal environment was investigated by Mahapatra and Panda [5]. Mahapatra et al. [6] studied the geometrically nonlinear transverse bending behavior of the shear-deformable laminated composite spherical shell panel under hygro-thermo-mechanical loading. Nonlinear free vibration behavior of laminated composite curved panel under hygrothermal environment was investigated by Mahapatra et al. [7]. Nonlinear flexural behavior of laminated composite doubly curved shell panel was investigated by Mahapatra et al. [8] under hygro-thermo-mechanical loading by considering the degraded composite material properties through a micromechanical model. Based on Grey Wolf algorithm, Kolahchi et al. [9] studied optimization of embedded piezoelectric sandwich nanocomposite plates for dynamic buckling analysis. Duc et al. [10] studied nonlinear dynamic response and vibration of imperfect functionally graded carbon nanotube-reinforced composite (FG-CNTRC) double-curved shallow shells based on analytical solution. In another work by Duc et al. [11–13], thermal and mechanical stabilities of FG-CNTRC truncated conical shells [11], static, dynamic and free vibration responses of FG-CNTRC rectangular plates surrounded on elastic foundations [12, 13] were investigated. They obtained the effective material properties of the structure through the rule of mixture. The geometrically nonlinear thermomechanical transverse deflection responses of the functionally graded curved structure under the influence of nonlinear thermal field were reported by Mahapatra et al. [14]. Kar et al. [15] investigated numerically the postbuckling load parameter of the functionally graded shell panels under uniform and non-uniform thermal environment using nonlinear finite element method. The frequency responses of free vibrated composite sandwich panel structure were investigated numerically by Katariya et al. [16] considering the geometrical nonlinearity via generalized Green–Lagrange strain kinematics in the framework of the equivalent single-layer theory. The vibration frequencies of multi-walled carbon nanotube-reinforced polymer composite structure were examined by Mehar et al. [17] via a generic higher order shear deformation kinematics for different panel geometries. The nonlinear eigen frequency response of the functionally graded single-walled carbon nanotube-reinforced sandwich structure was investigated by Mehar et al. [18] considering the Green–Lagrange nonlinear strain under uniform thermal environment. The vibration characteristics of carbon nanotube-reinforced sandwich curved shell panel were investigated by Mehar and Panda [19] under the elevated thermal environment. Electro-magneto wave propagation in piezoelectric sandwich plates made from nanocomposite core layer integrated with viscoelastic piezoelectric layers was presented by Kolahchi et al. [20].

Using Halpin–Tsai equations, Zarei et al. [21] investigated dynamic buckling of a sandwich truncated conical shell with polymer–carbon nanotube (CNT)–fiber multiphase nanocomposite layers. Hajmohammad et al. [22] presented the dynamic buckling behavior of a sandwich plate composed of laminated viscoelastic nanocomposite layers integrated with viscoelastic piezoelectric layers. The nonlinear static responses of the skew sandwich flat/curved shell panel including the corresponding stress values were examined by Katariya et al. [23] under the influence of the unvarying transverse mechanical load. Physics of the laminated composite plate with internal debonding was expressed by Hirwani et al. [24] mathematically via two kinds of mid-plane displacement functions based on Reddy’s simple shear deformation kinematic theory. The vibroacoustic responses of laminated composite curved panels subjected to harmonic point excitation in a combined temperature and moisture environment were investigated by Sharma et al. [25] numerically using a novel higher order finite-boundary element model. With respect to the development of the research works in the field of structures subjected to blast load and auxetic honeycomb materials, there are several works in the literature. A theoretical study was conducted by Qin et al. [26] to predict the large deflection response of fully clamped rectangular sandwich plates subjected to blast loading. The in-plane dynamic crushing behavior of re-entrant honeycomb was analyzed and compared by Hou et al. [27] with the conventional hexagon topology. The dynamic behavior of the delaminated composite plate subjected to blast loading was investigated by Hirwani et al. [28].

The response of multibody structures with plastic hinges subjected to confined blast loading was investigated by Ling et al. [29] through experimental tests, theoretical calculation and numerical simulation. Duc et al. [30–34] studied many works in the mentioned field. He and co-authors studied dynamic response and vibration of different structures such as composite double-curved shallow shells with auxetic honeycomb core [30], sandwich auxetic composite cylindrical panels [31], imperfect functionally graded CNT-reinforced composite double-curved shallow shells [32], imperfect functionally graded material (FGM) thick plates [33] and sandwich plates with negative Poisson’s ratio in auxetic honeycombs [34].

To the best of the authors’ knowledge, the blast analysis of sandwich plates with auxetic honeycombs and multiphase nanocomposite facesheets cannot be found in the literature. However, in this paper, dynamic response of viscoelastic nanocomposite sandwich plates resting on orthotropic viscoelastic foundation subjected to blast load is presented. The core of the sandwich plates is auxetic honeycombs and the facesheets are polymer reinforced by carbon fibers and CNTs. The structure is subjected to magnetic field and hygrothermal load. The viscoelastic property of the structure

is taken into account to achieve the realistic simulation based on Kelvin–Voigt model. The RZT is used for accurate simulation and considering the continuity boundary condition between layers. DCM and Newmark method are applied for solution of the motion equation to obtain the dynamic deflection of the sandwich structure. The effect of various parameters such as blast load, viscoelastic foundation, structural damping, magnetic field, volume fraction of CNTs, temperature and moisture changes, geometrical parameters of honeycomb layer and sandwich plate are examined on the dynamic deflection of the structure.

2 Schematic of sandwich plate and auxetic honeycomb cell

Figure 1 shows a sandwich plate with auxetic honeycomb core and multiphase nanocomposite facesheets where the Cartesian coordinate system (x, y, z) is located at the mid-plane of the core layer. The geometrical parameters of plates, length a , plate width b , thickness of core layer h_c , thickness of the top layer h_t and thickness of bottom layer h_b , are considered. The structure is located in orthotropic visco-Pasternak foundation with spring, shear and damper elements. The structure is subjected to magnetic field, blast load, temperature and moisture changes. The unit cells of the core are shown in Fig. 2 where the geometrical parameters of length of the inclined cell rib l , the length of the vertical cell rib d , and inclined angle, θ are indicated.

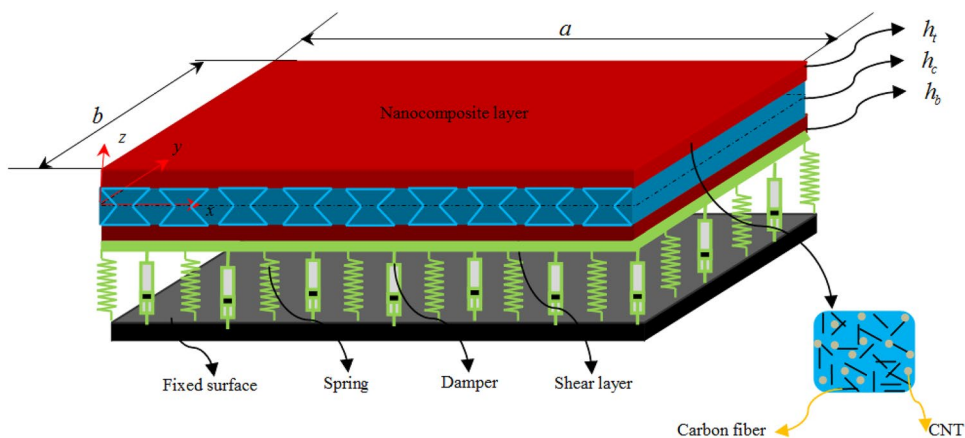
3 Refined zigzag theory

Based on the refined zigzag theory, the displacement fields can be written as follows [35]:

$$u_1^k(x, y, z, t) = u(x, y, t) + z\theta_x(x, y, t) + \Upsilon_x^k(z)\psi_x(x, y, t), \quad (1)$$

$$u_2^k(x, y, z, t) = v(x, y, t) + z\theta_y(x, y, t) + \Upsilon_y^k(z)\psi_y(x, y, t), \quad (2)$$

Fig. 1 A sandwich plate with auxetic honeycomb core and multiphase nanocomposite facesheets resting on orthotropic visco-Pasternak foundation



$$u_3^k(x, y, z, t) = w(x, y, t), \quad (3)$$

where superscript (k) shows the first layer [bottom (b)], second layer [core (c)] and third layer [top (t)]; u, v and w describe the displacements of mid-plane along x, y - and z -directions, respectively; θ_x and θ_y indicate the average bending rotations around the x - and y -axes, respectively; ψ_x and ψ_y present the spatial amplitudes of the zigzag rotation; Υ_x^k and Υ_y^k show the zigzag functions which are [35]

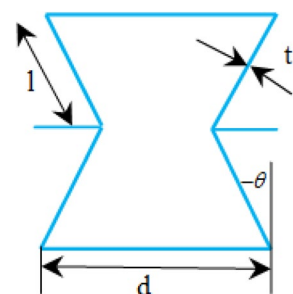
$$\Upsilon_x^b = (z + h) \left(\frac{G_x}{C_{11}^b} - 1 \right), \quad (4)$$

$$\Upsilon_y^b = (z + h) \left(\frac{G_y}{C_{22}^b} - 1 \right), \quad (5)$$

$$\Upsilon_x^c = (z + h) \left(\frac{G_x}{C_{11}^c} - 1 \right) + 2h_b \left(\frac{G_x}{C_{11}^b} - \frac{G_x}{C_{11}^c} \right), \quad (6)$$

$$\Upsilon_y^c = (z + h) \left(\frac{G_y}{C_{22}^c} - 1 \right) + 2h_b \left(\frac{G_y}{C_{22}^b} - \frac{G_y}{C_{22}^c} \right), \quad (7)$$

Fig. 2 Geometrical parameters of the honeycomb core layer cell



$$\Upsilon_x^t = (z + h) \left(\frac{G_x}{C_{11}^t} - 1 \right) + 2h_b \left(\frac{G_x}{C_{11}^b} - \frac{G_x}{C_{11}^c} \right) + 2h_c \left(\frac{G_x}{C_{11}^c} - \frac{G_x}{C_{11}^t} \right), \tag{8}$$

$$\Upsilon_y^t = (z + h) \left(\frac{G_y}{C_{22}^t} - 1 \right) + 2h_b \left(\frac{G_y}{C_{22}^b} - \frac{G_y}{C_{22}^c} \right) + 2h_c \left(\frac{G_y}{C_{22}^c} - \frac{G_y}{C_{22}^t} \right), \tag{9}$$

where C_{11}^k and C_{22}^k are elastic constants of layers. Using the above relations, the strain–displacement equations can be written as

$$\epsilon_{xx}^k = \frac{\partial u}{\partial x} + z \frac{\partial \theta_x}{\partial x} + \Upsilon_x^k \frac{\partial \psi_x}{\partial x}, \tag{10}$$

$$\epsilon_{yy}^k = \frac{\partial v}{\partial y} + z \frac{\partial \theta_y}{\partial y} + \Upsilon_y^k \frac{\partial \psi_y}{\partial y}, \tag{11}$$

$$\gamma_{xy}^k = \frac{\partial u}{\partial y} + \frac{\partial v}{\partial x} + z \left(\frac{\partial \theta_x}{\partial y} + \frac{\partial \theta_y}{\partial x} \right) + \Upsilon_x^k \frac{\partial \psi_x}{\partial y} + \Upsilon_y^k \frac{\partial \psi_y}{\partial x}, \tag{12}$$

$$\gamma_{xz}^k = \frac{\partial w}{\partial x} + \theta_x + \frac{\partial \Upsilon_x^k}{\partial z} \psi_x, \tag{13}$$

$$\gamma_{yz}^k = \frac{\partial w}{\partial y} + \theta_y + \frac{\partial \Upsilon_y^k}{\partial z} \psi_y. \tag{14}$$

4 Stress–strain relation

In this section, the stress–strain relations for the auxetic honeycomb core layer and nanocomposite facesheets are presented.

4.1 Auxetic honeycomb core layer

The stress–strain relation for the auxetic honeycomb core layer can be written as

$$\begin{bmatrix} \sigma_{xx}^c \\ \sigma_{yy}^c \\ \sigma_{yz}^c \\ \sigma_{xz}^c \\ \sigma_{xy}^c \end{bmatrix} = \begin{bmatrix} C_{11}^c & C_{12}^c & 0 & 0 & 0 \\ C_{21}^c & C_{22}^c & 0 & 0 & 0 \\ 0 & 0 & C_{44}^c & 0 & 0 \\ 0 & 0 & 0 & C_{55}^c & 0 \\ 0 & 0 & 0 & 0 & C_{66}^c \end{bmatrix} \begin{bmatrix} \epsilon_{xx}^c \\ \epsilon_{yy}^c \\ \gamma_{yz}^c \\ \gamma_{xz}^c \\ \gamma_{xy}^c \end{bmatrix}, \tag{15}$$

where the elastic constants can be defined as

$$\begin{aligned} C_{11}^c &= \frac{E_{11}^c}{1 - \nu_{12}^c \nu_{21}^c}, C_{12}^c = \frac{E_{11}^c \nu_{12}^c}{1 - \nu_{12}^c \nu_{21}^c}, C_{21}^c = \frac{E_{22}^c \nu_{21}^c}{1 - \nu_{12}^c \nu_{21}^c}, \\ C_{22}^c &= \frac{E_{22}^c}{1 - \nu_{12}^c \nu_{21}^c}, C_{44}^c = G_{23}^c, C_{55}^c = G_{13}^c, C_{66}^c = G_{12}^c, \end{aligned} \tag{16}$$

where [33]

$$\begin{aligned} E_{11}^c &= E^c \left(\frac{t}{l} \right)^3 \frac{\cos \theta}{\left(\frac{d}{l} + \sin \theta \right) \sin^2 \theta}, \quad E_{22}^c = E^c \left(\frac{t}{l} \right)^3 \frac{\left(\frac{d}{l} + \sin \theta \right)}{\cos^3 \theta}, \\ \nu_{12}^c &= \frac{\cos^2 \theta}{\left(\frac{d}{l} + \sin \theta \right) \sin \theta}, \quad G_{12}^c = E^c \left(\frac{t}{l} \right)^3 \frac{\left(\frac{d}{l} + \sin \theta \right)}{\left(\frac{d}{l} \right)^2 \left(1 + 2 \frac{d}{l} \right) \cos \theta}, \\ G_{13}^c &= G^c \left(\frac{t}{l} \right) \frac{\cos \theta}{\frac{d}{l} + \sin \theta}, \quad G_{23}^c = G^c \left(\frac{t}{l} \right) \frac{1 + 2 \sin^2 \theta}{2 \cos \theta \left(\frac{d}{l} + \sin \theta \right)}, \\ \rho^c &= \rho \left(\frac{t}{l} \right) \frac{\left(\frac{d}{l} + 2 \right)}{2 \cos \theta \left(\frac{d}{l} + \sin \theta \right)}, \end{aligned} \tag{17}$$

where E^c , G^c and ρ^c are the core Young’s moduli, shear moduli and mass density of the origin material, respectively.

4.2 Nanocomposite facesheets

The stress–strain relation for the nanocomposite face sheets can be written as

$$\begin{bmatrix} \sigma_{xx}^{t,b} \\ \sigma_{yy}^{t,b} \\ \sigma_{yz}^{t,b} \\ \sigma_{xz}^{t,b} \\ \sigma_{xy}^{t,b} \end{bmatrix} = \begin{bmatrix} C_{11}^{t,b} & C_{12}^{t,b} & 0 & 0 & 0 \\ C_{12}^{t,b} & C_{22}^{t,b} & 0 & 0 & 0 \\ 0 & 0 & C_{44}^{t,b} & 0 & 0 \\ 0 & 0 & 0 & C_{55}^{t,b} & 0 \\ 0 & 0 & 0 & 0 & C_{66}^{t,b} \end{bmatrix} \begin{bmatrix} \epsilon_{xx}^{t,b} - \alpha_{xx}^{t,b} \Delta T - \beta_{xx}^{t,b} \Delta C \\ \epsilon_{yy}^{t,b} - \alpha_{yy}^{t,b} \Delta T - \beta_{yy}^{t,b} \Delta C \\ \gamma_{yz}^{t,b} \\ \gamma_{xz}^{t,b} \\ \gamma_{xy}^{t,b} \end{bmatrix}, \tag{18}$$

where $\alpha_{xx}^{t,b}$, $\alpha_{yy}^{t,b}$ and $\beta_{xx}^{t,b}$, $\beta_{yy}^{t,b}$ are thermal expansion and moisture coefficients, respectively and elastic constants can be expanded as

$$C_{11}^{t,b} = C_{22}^{t,b} = \frac{E^{t,b}}{1 - (\nu^{t,b})^2}, C_{12}^{t,b} = \frac{E^{t,b}}{1 - (\nu^{t,b})^2}, C_{44}^{t,b} = C_{55}^{t,b} = C_{66}^{t,b} = G^{t,b}, \tag{19}$$

where the Young’s moduli and shear moduli of the facesheets can be obtained by Halpin–Tsai model.

5 Halpin–Tsai model

Here, the facesheets are reinforced by carbon fibers and CNTs. However, the equivalent material properties of the facesheets can be calculated by Halpin–Tsai model [36] as follows:

$$E_{11} = V_F E_{11}^F + V_{MNC} E^{MNC}, \tag{20}$$

$$\frac{1}{E_{22}} = \frac{1}{E_{22}^F} + \frac{V_{MNC}}{E^{MNC}} - V_F V_{MNC} - \frac{\frac{v_F E^{MNC}}{E_{22}^F} + \frac{v_{MNC}^2 E_{22}^F}{E^{MNC}} - 2v_F v_{MNC}}{V_F E_{22}^F + V_{MNC} E^{MNC}}, \tag{21}$$

$$\frac{1}{G_{12}} = \frac{V_F}{G_{12}^F} + \frac{V_{MNC}}{G^{MNC}}, \tag{22}$$

$$\rho = V_F \rho^F + V_{MNC} \rho^{MNC}, \tag{23}$$

$$v_{12} = V_F v^F + V_{MNC} v^{MNC}, \tag{24}$$

where E, G, ρ, V and ν are, respectively, Young’s modulus, shear modulus, mass density, volume fractions and Poisson’s ratio. The superscript or subscript F and MNC are related to the fibers and matrix of nanocomposite, respectively. However, the elastic modulus of nanocomposite can be expressed as

$$E^{MNC} = \frac{E^M}{8} \left[5 \left(\frac{1 + 2\beta_{dd} V_{CN}}{1 - \beta_{dd} V_{CN}} \right) + 3 \left(\frac{1 + 2(\ell^{CN}/d^{CN})\beta_{dl} V_{CN}}{1 - \beta_{dl} V_{CN}} \right) \right], \tag{25}$$

where

$$\beta_{dl} = \left(\frac{(E_{11}^{CN}/E^M) - (d^{CN}/4t^{CN})}{(E_{11}^{CN}/E^M) + (\ell^{CN}/2t^{CN})} \right), \tag{26}$$

$$\beta_{dd} = \left(\frac{(E_{11}^{CN}/E^M) - (d^{CN}/4t^{CN})}{(E_{11}^{CN}/E^M) + (d^{CN}/2t^{CN})} \right), \tag{27}$$

where E^M and V_M are Young’s modulus and volume fraction of the matrix, respectively; $E^{CN}, t^{CN}, d^{CN}, \ell^{CN}$ and V_{CN} represent, respectively, the Young’s modulus, thickness, outer diameter, length and volume fraction of CNTs which can be defined as

$$V_{CN} = \frac{w_{CN}}{w_{CN} + (\rho^{CN}/\rho^m) - (\rho^{CN}/\rho^m)w_{CN}}, \tag{28}$$

where w_{CN}, ρ^m and ρ^{CN} are mass fraction of CNTs, density of matrix and CNTs, respectively. The Poisson’s ratio and mass density of the MNC can be given as

$$v^{MNC} = v^M, \tag{29}$$

$$\rho^{MNC} = V_{CN} \rho^{CN} + V_M \rho^M, \tag{30}$$

$$G^{MNC} = \frac{E^{MNC}}{2(1 + v^{MNC})}, \tag{31}$$

where v^M and v^{MNC} are Poisson’s ratio of the matrix and MNC, respectively. Noted that due to the small amount of CNTs, the Poisson’s ratio of the matrix and MNC are considered equal [36]. The longitudinal and transverse thermal expansion coefficients can be expressed as

$$\alpha_x = \frac{V_F E_{11}^F \alpha_{11}^F + V_{MNC} E^{MNC} \alpha^{MNC}}{V_F E_{11}^F + V_{MNC} E^{MNC}}, \tag{32}$$

$$\alpha_\theta = (1 + v_{12}^F) V_F \alpha_{22}^F + (1 + v^{MNC}) V_{MNC} \alpha^{MNC} - v_{12} \alpha_x, \tag{33}$$

where α_{11}^F and α_{22}^F are the fiber thermal expansions and α^{MNC} is the thermal expansion of MNC which can be given as

$$\alpha^{MNC} = \frac{1}{2} \left\{ \left(\frac{V_{CN} E^{CN} \alpha^{CN} + V_M E^M \alpha^M}{V_{CN} E^{CN} + V_M E^M} \right) (1 - v^{MNC}) \right\} + \left((1 + v^M) \alpha^M V_M + (1 + v^M) \alpha^{CN} V_{CN} \right) \tag{34}$$

where α^{CN} and α^M are thermal expansion coefficients of CNTs and matrix, respectively. Since the matrix absorbs all the water content, the effect of moisture on the CNTs or fiber can be neglected [37]. However, the moisture coefficients of the nanocomposite may be stated as

$$\beta_x = \frac{V_F E_{11}^F + V_{MNC} E^{MNC} \beta^M}{V_F E_{11}^F + V_{MNC} E^{MNC}}, \tag{35}$$

$$\beta_\theta = (1 + v^{MNC}) V_{MNC} \beta^M - v_{12} \beta_x, \tag{36}$$

where β^M is the moisture coefficient of matrix. The temperature and moisture distributions are considered as

$$T = T_0 + \Delta T, \tag{37}$$

$$C = C_0 + \Delta C, \tag{38}$$

where ΔT and ΔC are temperature and moisture changes, respectively; T_0 and H_0 show the reference temperature and moisture concentration, respectively.

6 Energy method

In the energy method, three energies of potential, kinetic and work done by external forces should be calculated.

6.1 Potential energy

Using Eqs. (1)–(3), the total potential energy of the structure can be expressed as

$$\begin{aligned}
 U = & \frac{1}{2} \int_A \left(N_x \left(\frac{\partial u}{\partial x} + \frac{1}{2} \left(\frac{\partial w}{\partial x} \right)^2 \right) + M_x \frac{\partial \theta_x}{\partial x} + M_x^f \frac{\partial \psi_x}{\partial x} \right. \\
 & + N_y \left(\frac{\partial v}{\partial y} + \frac{1}{2} \left(\frac{\partial w}{\partial y} \right)^2 \right) + M_y \frac{\partial \theta_y}{\partial y} + M_y^f \frac{\partial \psi_y}{\partial y} \\
 & + N_{xy} \left(\frac{\partial u}{\partial y} + \frac{\partial v}{\partial x} + \left(\frac{\partial w}{\partial x} \frac{\partial w}{\partial y} \right) \right) \\
 & + M_{xy} \left(\frac{\partial \theta_x}{\partial y} + \frac{\partial \theta_y}{\partial x} \right) + M_{xy}^f \frac{\partial \psi_x}{\partial y} \\
 & + M_{yx}^f \frac{\partial \psi_y}{\partial x} + Q_x \left(\frac{\partial w}{\partial x} + \theta_x \right) \\
 & \left. + Q_x^f \psi_x + Q_y \left(\frac{\partial w}{\partial y} + \theta_y \right) + Q_y^f \psi_y \right) dA, \tag{39}
 \end{aligned}$$

where the resultant forces, moments and transverse shear stresses may be defined as

$$\begin{aligned}
 (N_x, N_y, N_{xy}) = & \int_{-h_b-h_c/2}^{-h_c/2} (\sigma_{xx}^b, \sigma_{yy}^b, \sigma_{xy}^b) dz \\
 & + \int_{-h_c/2}^{h_c/2} (\sigma_{xx}^c, \sigma_{yy}^c, \sigma_{xy}^c) dz + \int_{h_c/2}^{h_c/2+h_t} (\sigma_{xx}^t, \sigma_{yy}^t, \sigma_{xy}^t) dz, \tag{40}
 \end{aligned}$$

$$\begin{aligned}
 (M_x, M_y, M_{xy}) = & \int_{-h_b-h_c/2}^{-h_c/2} (\sigma_{xx}^b, \sigma_{yy}^b, \sigma_{xy}^b) z dz + \\
 & \int_{-h_c/2}^{h_c/2} (\sigma_{xx}^c, \sigma_{yy}^c, \sigma_{xy}^c) z dz + \\
 & \int_{h_c/2}^{h_c/2+h_t} (\sigma_{xx}^t, \sigma_{yy}^t, \sigma_{xy}^t) z dz, \tag{41}
 \end{aligned}$$

$$\begin{aligned}
 (M_x^Y, M_y^Y, M_{xy}^Y, M_{yx}^Y) = & \int_{-h_b-h_c/2}^{-h_c/2} (\Upsilon_x^b \sigma_{xx}^b, \Upsilon_y^b \sigma_{yy}^b, \Upsilon_x^b \sigma_{xy}^b, \Upsilon_y^b \sigma_{xy}^b) z dz + \\
 & \int_{-h_c/2}^{h_c/2} (\Upsilon_x^c \sigma_{xx}^c, \Upsilon_y^c \sigma_{yy}^c, \Upsilon_x^c \sigma_{xy}^c, \Upsilon_y^c \sigma_{xy}^c) z dz \\
 & + \int_{h_c/2}^{h_c/2+h_t} (\Upsilon_x^t \sigma_{xx}^t, \Upsilon_y^t \sigma_{yy}^t, \Upsilon_x^t \sigma_{xy}^t, \Upsilon_y^t \sigma_{xy}^t) z dz, \tag{42}
 \end{aligned}$$

$$\begin{aligned}
 (Q_x, Q_y) = & \int_{-h_b-h_c/2}^{-h_c/2} (\sigma_{xz}^b, \sigma_{yz}^b) dz + \\
 & \int_{-h_c/2}^{h_c/2} (\sigma_{xz}^c, \sigma_{yz}^c) dz + \int_{h_c/2}^{h_c/2+h_t} (\sigma_{xz}^t, \sigma_{yz}^t) dz, \tag{43}
 \end{aligned}$$

$$\begin{aligned}
 (Q_x^Y, Q_y^Y) = & \int_{-h_b-h_c/2}^{-h_c/2} \left(\frac{\partial \Upsilon_x^b}{\partial z} \sigma_{xz}^b, \frac{\partial \Upsilon_y^b}{\partial z} \sigma_{yz}^b \right) dz \\
 & + \int_{-h_c/2}^{h_c/2} \left(\frac{\partial \Upsilon_x^c}{\partial z} \sigma_{xz}^c, \frac{\partial \Upsilon_y^c}{\partial z} \sigma_{yz}^c \right) dz \\
 & + \int_{h_c/2}^{h_c/2+h_t} \left(\frac{\partial \Upsilon_x^t}{\partial z} \sigma_{xz}^t, \frac{\partial \Upsilon_y^t}{\partial z} \sigma_{yz}^t \right) dz. \tag{44}
 \end{aligned}$$

6.2 Kinetic energy

Using Eqs. (1)–(3), the kinetic energy of the sandwich structure can be expressed as

$$\begin{aligned}
 K_{total} = & \frac{1}{2} \int_A [I_0 (\dot{u}^2 + \dot{v}^2 + \dot{w}^2) + I_1 (2i\dot{\theta}_x + 2\dot{v}\dot{\theta}_y) \\
 & + I_2 (\dot{\theta}_x^2 + \dot{\theta}_y^2) + I_0^{Y_x} (2i\dot{\psi}_x) \\
 & + I_0^{Y_y} (2\dot{v}\dot{\psi}_y) + I_1^{Y_x} (2\dot{\theta}_x \dot{\psi}_x) + I_1^{Y_x} (2\dot{\theta}_x \dot{\psi}_x) \\
 & + I_1^{Y_y} (+2\dot{\theta}_y \dot{\psi}_y) + I_2^{Y_x} (\dot{\psi}_x^2) + I_2^{Y_y} (\dot{\psi}_y^2)] dA, \tag{45}
 \end{aligned}$$

where the mass moments of inertia can be defined as below:

$$\begin{aligned}
 (I_0, I_1, I_2, I_0^Y, I_1^Y, I_2^Y) = & \int_{-h_b-h_c/2}^{-h_c/2} \rho^b (1, z, z^2, \Upsilon_j^b, z\Upsilon_j^b, (\Upsilon_j^b)^2) dz \\
 & + \int_{-h_c/2}^{h_c/2} \rho^c (1, z, z^2, \Upsilon_j^c, z\Upsilon_j^c, (\Upsilon_j^c)^2) dz \\
 & + \int_{h_c/2}^{h_c/2+h_t} \rho^t (1, z, z^2, \Upsilon_j^t, z\Upsilon_j^t, (\Upsilon_j^t)^2) dz \quad j = x, y. \tag{46}
 \end{aligned}$$

6.3 External works

The applied external works due to the viscoelastic medium, magnetic field, hygrothermal environment and blast load can be expressed as

$$W = -\frac{1}{2} \int_A (q_v + q_m + q_h + q_b) u_3 dA. \tag{47}$$

6.3.1 Orthotropic visco-Pasternak medium

The external force due to the orthotropic visco-Pasternak medium can be expressed as [9]

$$q_v = k_w u_3 + c_d \dot{u}_3 - k_{g1} \left(\cos^2 \varphi \frac{\partial^2 u_3}{\partial x^2} + 2 \cos \varphi \sin \varphi \frac{\partial^2 u_3}{\partial x \partial y} + \sin^2 \varphi \frac{\partial^2 u_3}{\partial y^2} \right) - k_{g2} \left(\sin^2 \varphi \frac{\partial^2 u_3}{\partial x^2} - 2 \sin \varphi \cos \varphi \frac{\partial^2 u_3}{\partial x \partial y} + \cos^2 \varphi \frac{\partial^2 u_3}{\partial y^2} \right), \tag{48}$$

where angle φ denotes is the orthotropic foundation angle with respect to the global; k_w , c_d , k_{g1} and k_{g2} are normal spring, damping and shear constants, respectively.

6.3.2 Magnetic field

Assuming the 2D magnetic field as $H_0 = H_x \delta_{x\theta} \hat{e}_x + H_y \delta_{y\theta} \hat{e}_y$, the Lorentz force in the facesheets can be obtained as [21]

$$f_m = \eta \underbrace{\left(\nabla \times (\nabla \times (u \times H_0)) \right)}_J \times H_0, \tag{49}$$

in which η is the magnetic field permeability, ∇ indicates the gradient operator, $u = (u_1^{t,b}, u_2^{t,b}, u_3^{t,b})$ denotes the displacement field vector, h represents the distributing vector of magnetic field, and J is the current density. Substituting Eqs. (1)–(3) into Eq. (49) yields

$$f_x = \eta H_y^2 \left[\left(\frac{\partial^2 u}{\partial x^2} + \frac{\partial^2 u}{\partial y^2} \right) + z \left(\frac{\partial^2 \theta_x}{\partial x^2} + \frac{\partial^2 \theta_x}{\partial y^2} \right) + \Upsilon_x^{t,b} \left(\frac{\partial^2 \psi_x}{\partial x^2} + \frac{\partial^2 \psi_x}{\partial y^2} \right) \right], \tag{50}$$

$$f_y = \eta H_x^2 \left[\left(\frac{\partial^2 v}{\partial x^2} + \frac{\partial^2 v}{\partial y^2} \right) + z \left(\frac{\partial^2 \theta_y}{\partial x^2} + \frac{\partial^2 \theta_y}{\partial y^2} \right) + \Upsilon_y^{t,b} \left(\frac{\partial^2 \psi_y}{\partial x^2} + \frac{\partial^2 \psi_y}{\partial y^2} \right) \right], \tag{51}$$

$$f_z = \eta \left[H_y^2 \left(\frac{\partial \theta_x}{\partial x} + \frac{\partial^2 w}{\partial y^2} \right) + H_x^2 \left(\frac{\partial \theta_y}{\partial y} + \frac{\partial^2 w}{\partial x^2} \right) \right]. \tag{52}$$

The resultant force and bending moments can be obtained as below:

$$(F_{xm}, F_{ym}, F_{zm}) = \int_{-h_b-h_c/2}^{-h_c/2} (f_x^b, f_y^b, f_z^b) dz + \int_{h_c/2}^{h_c/2+h_t} (f_x^t, f_y^t, f_z^t) dz, \tag{53}$$

$$(M_{xm}, M_{ym}, M_{zm}) = \int_{-h_b-h_c/2}^{-h_c/2} (f_x^b, f_y^b, f_z^b) z dz + \int_{h_c/2}^{h_c/2+h_t} (f_x^t, f_y^t, f_z^t) z dz, \tag{54}$$

$$(M_{xm}^Y, M_{xm}^X, M_{ym}^X, M_{ym}^Y) = \int_{-h_b-h_c/2}^{-h_c/2} (f_x^b \Upsilon_x^b, f_x^b \Upsilon_y^b, f_y^b \Upsilon_x^b, f_y^b \Upsilon_y^b) z dz + \int_{h_c/2}^{h_c/2+h_t} (f_x^t \Upsilon_x^t, f_x^t \Upsilon_y^t, f_y^t \Upsilon_x^t, f_y^t \Upsilon_y^t) z dz. \tag{55}$$

6.3.3 Hygrothermal environment

The internal force due to the thermal and moisture loads can be expressed as

$$q_h = \int \left[\frac{N_x^H}{2} \left(\frac{\partial w}{\partial x} \right)^2 + \frac{N_y^H}{2} \left(\frac{\partial w}{\partial y} \right)^2 \right] dA. \tag{56}$$

In the above relations, N_x^H and N_y^H are

$$N_x^H = - \int_{-h_b-h_c/2}^{-h_c/2} \left[(C_{11}^b \alpha_{xx}^b + C_{12}^b \alpha_{yy}^b) \Delta T + (C_{11}^b \beta_{xx}^b + C_{12}^b \beta_{yy}^b) \Delta C \right] dz - \int_{-h_b-h_c/2}^{-h_c/2} \left[(C_{11}^t \alpha_{xx}^t + C_{12}^t \alpha_{yy}^t) \Delta T + (C_{11}^t \beta_{xx}^t + C_{12}^t \beta_{yy}^t) \Delta C \right] dz, \tag{57}$$

$$N_y^H = - \int_{-h_b-h_c/2}^{-h_c/2} \left[(C_{12}^b \alpha_{xx}^b + C_{22}^b \alpha_{yy}^b) \Delta T + (C_{12}^b \beta_{xx}^b + C_{22}^b \beta_{yy}^b) \Delta C \right] dz - \int_{-h_b-h_c/2}^{-h_c/2} \left[(C_{12}^t \alpha_{xx}^t + C_{22}^t \alpha_{yy}^t) \Delta T + (C_{12}^t \beta_{xx}^t + C_{22}^t \beta_{yy}^t) \Delta C \right] dz. \tag{58}$$

6.3.4 Blast load

The blast wave pressure is considered to be uniformly applied to the plate. The force done by the blast load can be expressed as [32]

$$P_{\text{blast}} = 1.8 P_{S0} \left[1 - \frac{t}{T_s} \right] \exp \left\{ \frac{-at}{T_s} \right\}, \tag{59}$$

where “1.8” is a factor for considering the hemispherical blast, a is wave decay coefficient, P_{S0} is the maximum pressure of blast and T_s is the parameter of duration of the blast pulse which can be expressed as [38–40]

$$P_{S0} = 0.085 \left(\frac{1}{Z} \right) + 0.3 \left(\frac{1}{Z} \right)^2 + 0.8 \left(\frac{1}{Z} \right)^3, \tag{60}$$

$$T_s = 1.2 \sqrt[6]{W} \sqrt{R}, \tag{61}$$

$$a = Z^2 - 3.7Z + 4.2, \tag{62}$$

where P_0 is atmosphere pressure and Z is

$$Z = \frac{R}{W^{0.33}}, \tag{63}$$

where R is the distance of center of blast to center of the structure and W is the mass of explosive materials in terms of TNT.

7 Motion equations

Employing Hamilton’s principle, the equations of motion can be derived as below:

$$\delta u : \frac{\partial N_x}{\partial x} + \frac{\partial N_{xy}}{\partial y} = I_0 \frac{\partial^2 u}{\partial t^2} + I_1 \frac{\partial^2 \theta_x}{\partial t^2} + I_0^{\gamma_x} \frac{\partial^2 \psi_x}{\partial t^2} - F_{xm}, \tag{64}$$

$$\delta v : \frac{\partial N_{xy}}{\partial x} + \frac{\partial N_y}{\partial y} = I_0 \frac{\partial^2 v}{\partial t^2} + I_1 \frac{\partial^2 \theta_y}{\partial t^2} + I_0^{\gamma_y} \frac{\partial^2 \psi_y}{\partial t^2} - F_{ym}, \tag{65}$$

$$\delta w : \frac{\partial Q_x}{\partial x} + \frac{\partial Q_y}{\partial y} + \frac{\partial}{\partial x} \left(N^H \frac{\partial w}{\partial x} \right) + \frac{\partial}{\partial y} \left(N_y^H \frac{\partial w}{\partial y} \right) - q_v - q_h - q_b = I_0 \frac{\partial^2 w}{\partial t^2} - F_{zm}, \tag{66}$$

$$\delta \theta_x : \frac{\partial M_x}{\partial x} + \frac{\partial M_{xy}}{\partial y} - Q_x = I_1 \frac{\partial^2 u}{\partial t^2} + I_2 \frac{\partial^2 \theta_x}{\partial t^2} + I_1^{\gamma_x} \frac{\partial^2 \psi_x}{\partial t^2} - M_{xm}, \tag{67}$$

$$\delta \theta_y : \frac{\partial M_{xy}}{\partial x} + \frac{\partial M_y}{\partial y} - Q_y = I_1 \frac{\partial^2 v}{\partial t^2} + I_2 \frac{\partial^2 \theta_y}{\partial t^2} + I_1^{\gamma_y} \frac{\partial^2 \psi_y}{\partial t^2} - M_{ym}, \tag{68}$$

$$\delta \psi_x : \frac{\partial M_x^{\gamma}}{\partial x} + \frac{\partial M_{xy}^{\gamma}}{\partial y} - Q_x^{\gamma} = I_0^{\gamma_x} \frac{\partial^2 u}{\partial t^2} + I_1^{\gamma_x} \frac{\partial^2 \theta_x}{\partial t^2} + I_2^{\gamma_x} \frac{\partial^2 \psi_x}{\partial t^2} - M_{xm}^{\gamma} - M_{xm}^{\gamma}, \tag{69}$$

$$\delta \psi_y : \frac{\partial M_{yx}^{\gamma}}{\partial x} + \frac{\partial M_y^{\gamma}}{\partial y} - Q_y^{\gamma} = I_0^{\gamma_y} \frac{\partial^2 v}{\partial t^2} + I_1^{\gamma_y} \frac{\partial^2 \theta_y}{\partial t^2} + I_2^{\gamma_y} \frac{\partial^2 \psi_y}{\partial t^2} - M_{ym}^{\gamma} - M_{ym}^{\gamma}. \tag{70}$$

Substituting Eqs. (1)–(18) into Eqs. (40)–(44), considering structural damping using Kelvin–Voigt [41] theory

($C_{ij}^k = C_{ij}^k(1 + g\partial/\partial t)$) where g denotes the structural damping coefficient, the stress resultants can be obtained as

$$N_x = A_{11}^k \frac{\partial u}{\partial x} + B_{11}^k \frac{\partial \theta_x}{\partial x} + G_{11}^k \frac{\partial \psi_x}{\partial x} + A_{12}^k \frac{\partial v}{\partial y} + B_{12}^k \frac{\partial \theta_y}{\partial y} + H_{12}^k \frac{\partial \psi_y}{\partial y} + g \frac{\partial}{\partial t} \left(A_{11}^k \frac{\partial u}{\partial x} + B_{11}^k \frac{\partial \theta_x}{\partial x} + G_{11}^k \frac{\partial \psi_x}{\partial x} + A_{12}^k \frac{\partial v}{\partial y} + B_{12}^k \frac{\partial \theta_y}{\partial y} + H_{12}^k \frac{\partial \psi_y}{\partial y} \right), \tag{71}$$

$$N_y = A_{12}^k \frac{\partial u}{\partial x} + B_{12}^k \frac{\partial \theta_x}{\partial x} + G_{12}^k \frac{\partial \psi_x}{\partial x} + A_{22}^k \frac{\partial v}{\partial y} + B_{22}^k \frac{\partial \theta_y}{\partial y} + H_{22}^k \frac{\partial \psi_y}{\partial y} + g \frac{\partial}{\partial t} \left(A_{12}^k \frac{\partial u}{\partial x} + B_{12}^k \frac{\partial \theta_x}{\partial x} + G_{12}^k \frac{\partial \psi_x}{\partial x} + A_{22}^k \frac{\partial v}{\partial y} + B_{22}^k \frac{\partial \theta_y}{\partial y} + H_{22}^k \frac{\partial \psi_y}{\partial y} \right), \tag{72}$$

$$N_{xy} = A_{66}^k \left(\frac{\partial u}{\partial y} + \frac{\partial v}{\partial x} \right) + B_{66}^k \left(\frac{\partial \theta_x}{\partial y} + \frac{\partial \theta_y}{\partial x} \right) + G_{66}^k \frac{\partial \psi_x}{\partial y} + H_{66}^k \frac{\partial \psi_y}{\partial x} + g \frac{\partial}{\partial t} \left(A_{66}^k \left(\frac{\partial u}{\partial y} + \frac{\partial v}{\partial x} \right) + B_{66}^k \left(\frac{\partial \theta_x}{\partial y} + \frac{\partial \theta_y}{\partial x} \right) + G_{66}^k \frac{\partial \psi_x}{\partial y} + H_{66}^k \frac{\partial \psi_y}{\partial x} \right), \tag{73}$$

$$M_x = B_{11}^k \frac{\partial u}{\partial x} + D_{11}^k \frac{\partial \theta_x}{\partial x} + I_{11}^k \frac{\partial \psi_x}{\partial x} + B_{12}^k \frac{\partial v}{\partial y} + D_{12}^k \frac{\partial \theta_y}{\partial y} + J_{12}^k \frac{\partial \psi_y}{\partial y} + g \frac{\partial}{\partial t} \left(B_{11}^k \frac{\partial u}{\partial x} + D_{11}^k \frac{\partial \theta_x}{\partial x} + I_{11}^k \frac{\partial \psi_x}{\partial x} + B_{12}^k \frac{\partial v}{\partial y} + D_{12}^k \frac{\partial \theta_y}{\partial y} + J_{12}^k \frac{\partial \psi_y}{\partial y} \right), \tag{74}$$

$$M_y = B_{12}^k \frac{\partial u}{\partial x} + D_{12}^k \frac{\partial \theta_x}{\partial x} + I_{12}^k \frac{\partial \psi_x}{\partial x} + B_{22}^k \frac{\partial v}{\partial y} + D_{22}^k \frac{\partial \theta_y}{\partial y} + J_{22}^k \frac{\partial \psi_y}{\partial y} + g \frac{\partial}{\partial t} \left(B_{12}^k \frac{\partial u}{\partial x} + D_{12}^k \frac{\partial \theta_x}{\partial x} + I_{12}^k \frac{\partial \psi_x}{\partial x} + B_{22}^k \frac{\partial v}{\partial y} + D_{22}^k \frac{\partial \theta_y}{\partial y} + J_{22}^k \frac{\partial \psi_y}{\partial y} \right), \tag{75}$$

$$M_{xy} = B_{66}^k \left(\frac{\partial u}{\partial y} + \frac{\partial v}{\partial x} \right) + D_{66}^k \left(\frac{\partial \theta_x}{\partial y} + \frac{\partial \theta_y}{\partial x} \right) + I_{66}^k \frac{\partial \psi_x}{\partial y} + J_{66}^k \frac{\partial \psi_y}{\partial x} + g \frac{\partial}{\partial t} \left(B_{66}^k \left(\frac{\partial u}{\partial y} + \frac{\partial v}{\partial x} \right) + D_{66}^k \left(\frac{\partial \theta_x}{\partial y} + \frac{\partial \theta_y}{\partial x} \right) + I_{66}^k \frac{\partial \psi_x}{\partial y} + J_{66}^k \frac{\partial \psi_y}{\partial x} \right), \tag{76}$$

$$\begin{aligned}
 M_x^Y &= G_{11}^k \frac{\partial u}{\partial x} + I_{11}^k \frac{\partial \theta_x}{\partial x} + K_{11}^k \frac{\partial \psi_x}{\partial x} + G_{12}^k \frac{\partial v}{\partial y} \\
 &+ I_{12}^k \frac{\partial \theta_y}{\partial y} + L_{12}^k \frac{\partial \psi_y}{\partial y} + g \frac{\partial}{\partial t} \left(G_{11}^k \frac{\partial u}{\partial x} + I_{11}^k \frac{\partial \theta_x}{\partial x} \right. \\
 &\left. + K_{11}^k \frac{\partial \psi_x}{\partial x} + G_{12}^k \frac{\partial v}{\partial y} + I_{12}^k \frac{\partial \theta_y}{\partial y} + L_{12}^k \frac{\partial \psi_y}{\partial y} \right), \tag{77}
 \end{aligned}$$

$$\begin{aligned}
 M_y^Y &= H_{12}^k \frac{\partial u}{\partial x} + J_{12}^k \frac{\partial \theta_x}{\partial x} + L_{12}^k \frac{\partial \psi_x}{\partial x} + H_{22}^k \frac{\partial v}{\partial y} \\
 &+ J_{22}^k \frac{\partial \theta_y}{\partial y} + M_{22}^k \frac{\partial \psi_y}{\partial y} + g \frac{\partial}{\partial t} \left(H_{12}^k \frac{\partial u}{\partial x} + J_{12}^k \frac{\partial \theta_x}{\partial x} \right. \\
 &\left. + L_{12}^k \frac{\partial \psi_x}{\partial x} + H_{22}^k \frac{\partial v}{\partial y} + J_{22}^k \frac{\partial \theta_y}{\partial y} + M_{22}^k \frac{\partial \psi_y}{\partial y} \right), \tag{78}
 \end{aligned}$$

$$\begin{aligned}
 M_{xy}^Y &= G_{66}^k \left(\frac{\partial u}{\partial y} + \frac{\partial v}{\partial x} \right) + I_{66}^k \left(\frac{\partial \theta_x}{\partial y} + \frac{\partial \theta_y}{\partial x} \right) \\
 &+ K_{66}^k \frac{\partial \psi_x}{\partial y} + L_{66}^k \frac{\partial \psi_y}{\partial x} + g \frac{\partial}{\partial t} \left(G_{66}^k \left(\frac{\partial u}{\partial y} + \frac{\partial v}{\partial x} \right) \right. \\
 &\left. + I_{66}^k \left(\frac{\partial \theta_x}{\partial y} + \frac{\partial \theta_y}{\partial x} \right) + K_{66}^k \frac{\partial \psi_x}{\partial y} + L_{66}^k \frac{\partial \psi_y}{\partial x} \right), \tag{79}
 \end{aligned}$$

$$\begin{aligned}
 M_{yx}^Y &= H_{66}^k \left(\frac{\partial u}{\partial y} + \frac{\partial v}{\partial x} \right) + J_{66}^k \left(\frac{\partial \theta_x}{\partial y} + \frac{\partial \theta_y}{\partial x} \right) \\
 &+ L_{66}^k \frac{\partial \psi_x}{\partial y} + M_{66}^k \frac{\partial \psi_y}{\partial x} + g \frac{\partial}{\partial t} \left(H_{66}^k \left(\frac{\partial u}{\partial y} + \frac{\partial v}{\partial x} \right) \right. \\
 &\left. + J_{66}^k \left(\frac{\partial \theta_x}{\partial y} + \frac{\partial \theta_y}{\partial x} \right) + L_{66}^k \frac{\partial \psi_x}{\partial y} + M_{66}^k \frac{\partial \psi_y}{\partial x} \right), \tag{80}
 \end{aligned}$$

$$Q_x = A_{55}^k \left(\frac{\partial w}{\partial x} + \theta_x \right) + N_{55}^k \psi_x + g \frac{\partial}{\partial t} \left(A_{55}^k \left(\frac{\partial w}{\partial x} + \theta_x \right) + N_{55}^k \psi_x \right), \tag{81}$$

$$Q_y = A_{44}^k \left(\frac{\partial w}{\partial y} + \theta_y \right) + O_{44}^k \psi_y + g \frac{\partial}{\partial t} \left(A_{44}^k \left(\frac{\partial w}{\partial y} + \theta_y \right) + O_{44}^k \psi_y \right), \tag{82}$$

$$Q_x^Y = N_{55}^k \left(\frac{\partial w}{\partial x} + \theta_x \right) + P_{55}^k \psi_x + g \frac{\partial}{\partial t} \left(N_{55}^k \left(\frac{\partial w}{\partial x} + \theta_x \right) + P_{55}^k \psi_x \right), \tag{83}$$

$$Q_y^Y = O_{44}^k \left(\frac{\partial w}{\partial y} + \theta_y \right) + Q_{44}^k \psi_y + g \frac{\partial}{\partial t} \left[O_{44}^k \left(\frac{\partial w}{\partial y} + \theta_y \right) + Q_{44}^k \psi_y \right], \tag{84}$$

where

$$A_{ij}^k = \int_{-h_b-h_c/2}^{-h_c/2} C_{ij}^k dz + \int_{-h_c/2}^{h_c/2} C_{ij}^k dz + \int_{h_c/2}^{h_c/2+h_t} C_{ij}^k dz, \tag{85}$$

$$B_{ij}^k = \int_{-h_b-h_c/2}^{-h_c/2} C_{ij}^k z dz + \int_{-h_c/2}^{h_c/2} C_{ij}^k z dz + \int_{h_c/2}^{h_c/2+h_t} C_{ij}^k z dz, \tag{86}$$

$$D_{ij}^k = \int_{-h_b-h_c/2}^{-h_c/2} C_{ij}^k z^2 dz + \int_{-h_c/2}^{h_c/2} C_{ij}^k z^2 dz + \int_{h_c/2}^{h_c/2+h_t} C_{ij}^k z^2 dz, \tag{87}$$

$$G_{ij}^k = \int_{-h_b-h_c/2}^{-h_c/2} C_{ij}^k Y_x dz + \int_{-h_c/2}^{h_c/2} C_{ij}^k Y_x dz + \int_{h_c/2}^{h_c/2+h_t} C_{ij}^k Y_x dz, \tag{88}$$

$$H_{ij}^k = \int_{-h_b-h_c/2}^{-h_c/2} C_{ij}^k Y_y dz + \int_{-h_c/2}^{h_c/2} C_{ij}^k Y_y dz + \int_{h_c/2}^{h_c/2+h_t} C_{ij}^k Y_y dz, \tag{89}$$

$$I_{ij}^k = \int_{-h_b-h_c/2}^{-h_c/2} C_{ij}^k Y_x z dz + \int_{-h_c/2}^{h_c/2} C_{ij}^k Y_x z dz + \int_{h_c/2}^{h_c/2+h_t} C_{ij}^k Y_x z dz, \tag{90}$$

$$J_{ij}^k = \int_{-h_b-h_c/2}^{-h_c/2} C_{ij}^k Y_y z dz + \int_{-h_c/2}^{h_c/2} C_{ij}^k Y_y z dz + \int_{h_c/2}^{h_c/2+h_t} C_{ij}^k Y_y z dz, \tag{91}$$

$$\begin{aligned}
 K_{ij}^k &= \int_{-h_b-h_c/2}^{-h_c/2} C_{ij}^k (Y_x)^2 dz + \int_{-h_c/2}^{h_c/2} C_{ij}^k (Y_x)^2 dz \\
 &+ \int_{h_c/2}^{h_c/2+h_t} C_{ij}^k (Y_x)^2 dz, \tag{92}
 \end{aligned}$$

$$L_{ij}^k = \int_{-h_b-h_c/2}^{-h_c/2} C_{ij}^k Y_x Y_y dz + \int_{-h_c/2}^{h_c/2} C_{ij}^k Y_x Y_y dz + \int_{h_c/2}^{h_c/2+h_t} C_{ij}^k Y_x Y_y dz, \tag{93}$$

$$\begin{aligned}
 M_{ij}^k &= \int_{-h_b-h_c/2}^{-h_c/2} C_{ij}^k (Y_y)^2 dz + \int_{-h_c/2}^{h_c/2} C_{ij}^k (Y_y)^2 dz \\
 &+ \int_{h_c/2}^{h_c/2+h_t} C_{ij}^k (Y_y)^2 dz, \tag{94}
 \end{aligned}$$

$$M_{55}^k = \int_{-h_b-h_c/2}^{-h_c/2} C_{ij}^k \frac{\partial Y_x}{\partial z} dz + \int_{-h_c/2}^{h_c/2} C_{ij}^k \frac{\partial Y_x}{\partial z} dz + \int_{h_c/2}^{h_c/2+h_t} C_{ij}^k \frac{\partial Y_x}{\partial z} dz, \tag{95}$$

$$P_{55}^k = \int_{-h_b-h_c/2}^{-h_c/2} C_{ij}^k \frac{\partial^2 Y_x}{\partial z^2} dz + \int_{-h_c/2}^{h_c/2} C_{ij}^k \frac{\partial^2 Y_x}{\partial z^2} dz + \int_{h_c/2}^{h_c/2+h_t} C_{ij}^k \frac{\partial^2 Y_x}{\partial z^2} dz, \tag{96}$$

$$O_{55}^k = \int_{-h_b-h_c/2}^{-h_c/2} C_{ij}^k \frac{\partial Y_y}{\partial z} dz + \int_{-h_c/2}^{h_c/2} C_{ij}^k \frac{\partial Y_y}{\partial z} dz + \int_{h_c/2}^{h_c/2+h_t} C_{ij}^k \frac{\partial Y_y}{\partial z} dz, \tag{97}$$

$$Q_{55}^k = \int_{-h_b-h_c/2}^{-h_c/2} C_{ij}^k \frac{\partial^2 Y_y}{\partial z^2} dz + \int_{-h_c/2}^{h_c/2} C_{ij}^k \frac{\partial^2 Y_y}{\partial z^2} dz + \int_{h_c/2}^{h_c/2+h_t} C_{ij}^k \frac{\partial^2 Y_y}{\partial z^2} dz. \tag{98}$$

Also, the boundary conditions are considered as below:

- Clamped supported at four surfaces

$$\begin{aligned} x = 0, a \Rightarrow u = v = w = \theta_x = \theta_y = \psi_x = \psi_y = 0, \\ y = 0, b \Rightarrow u = v = w = \theta_x = \theta_y = \psi_x = \psi_y = 0. \end{aligned} \tag{99}$$

- Simply supported at four surfaces

$$\begin{aligned} x = 0, a \Rightarrow v = w = \theta_y = \psi_y = M_y = M_y^Y = M_{xy} = 0, \\ y = 0, b \Rightarrow u = w = \theta_x = \psi_x = M_x = M_x^Y = M_{xy} = 0. \end{aligned} \tag{100}$$

- Clamped supported at two surfaces and simply supported at two another surfaces

$$\begin{aligned} x = 0, a \Rightarrow u = v = w = \theta_x = \theta_y = \psi_x = \psi_y = 0, \\ y = 0, b \Rightarrow u = w = \theta_x = \psi_x = M_x = M_x^Y = M_{xy} = 0. \end{aligned} \tag{101}$$

8 Solution method

8.1 DCM

DCM is a numerical procedure expressing a calculus operator (\mathfrak{R}) value of the function ($f(x, y)$) at a discrete point in the solution domain as a weighted linear sum of discrete function values chosen within the overall domain of a problem. For a two-dimensional problem, supposing that there are N arbitrarily located grid points, the cubature approximation at the i th discrete point can be expressed as [42]

$$\mathfrak{R}f(x, y)_i \approx \sum_{j=1}^N C_{ij}f(x_j, y_j), \tag{102}$$

where C_{ij} and N are the cubature weighting coefficients and total number of grid points in the solution domain, respectively. The computation of the weighting coefficients can be done using the following expression:

$$\begin{aligned} \mathfrak{R}\{x^{\nu-\mu}y^\mu\}_i = \sum_{j=1}^N C_{ij}f(x_j^{\nu-\mu}y_j^\mu), \quad \mu = 0, 1, 2, \dots, \nu, \\ \nu = 0, 1, 2, \dots, N - 1, \quad i = 1, 2, \dots, N. \end{aligned} \tag{103}$$

The above equation may be written in matrix form as

$$\begin{bmatrix} C_{i1} \\ C_{i2} \\ \vdots \\ C_{in} \end{bmatrix} \begin{bmatrix} x_j^{\nu-\mu}y_j^\mu \\ \vdots \\ \vdots \end{bmatrix} = [\mathfrak{R}\{x^{\nu-\mu}y^\mu\}_i]. \tag{104}$$

The coefficient matrix, $[x_j^{\nu-\mu}y_j^\mu]$, can be expanded with j

in column wise and one row of each pair of (ν, μ) . Also, each pair of (ν, μ) is required to fill the column on the right of the equal sign. The cubature weighting coefficients may be obtained by solving Eq. (104) repeatedly for $i = 1, 2, \dots, N$, respectively.

However, using DCM, the motion equations can be written in matrix form as

$$\begin{aligned} \begin{bmatrix} M_{bb} & M_{bd} \\ M_{db} & M_{dd} \end{bmatrix} \begin{bmatrix} \ddot{Y}_b \\ \ddot{Y}_d \end{bmatrix} + \begin{bmatrix} C_{bb} & C_{bd} \\ C_{db} & C_{dd} \end{bmatrix} \begin{bmatrix} \dot{Y}_b \\ \dot{Y}_d \end{bmatrix} \\ + \begin{bmatrix} K_{bb} & K_{bd} \\ K_{db} & K_{dd} \end{bmatrix} \begin{bmatrix} Y_b \\ Y_d \end{bmatrix} = \begin{bmatrix} 0 \\ Q_b \end{bmatrix}, \end{aligned} \tag{105}$$

in which $[K]$ denotes the stiffness matrix, $[C]$ is the damp matrix, $[M]$ is the mass matrix, $[Q_b]$ is the external blast load, $\{Y\} = \{u, v, w, \theta_x, \theta_y, \psi_x, \psi_y\}$ is the displacement vector; subscripts b and d indicate the boundary and domain points.

8.2 Newmark method

In this section, Newmark method [43] is applied in the time domain to obtain the time response of the structure under the blast loads. Based on this method, Eq. (105) can be written in the general form as below:

$$K^*(d_{i+1}) = Q_{i+1}, \tag{106}$$

where subscript $i + 1$ indicates the time $t = t_{i+1}$, $K^*(d_{i+1})$ and Q_{i+1} are the effective stiffness matrix and the effective load vector which can be considered as

$$K^*(d_{i+1}) = K_L + K_{NL}(d_{i+1}) + \alpha_0 M + \alpha_1 C, \tag{107}$$

$$Q_{i+1}^* = Q_{i+1} + M(\alpha_0 \dot{d}_i + \alpha_2 \ddot{d}_i + \alpha_3 \ddot{d}_i) + C(\alpha_1 \dot{d}_i + \alpha_4 \dot{d}_i + \alpha_5 \ddot{d}_i), \tag{108}$$

where [43]

$$\begin{aligned} \alpha_0 = \frac{1}{\chi \Delta t^2}, \quad \alpha_1 = \frac{\gamma}{\chi \Delta t}, \quad \alpha_2 = \frac{1}{\chi \Delta t}, \\ \alpha_3 = \frac{1}{2\chi} - 1, \quad \alpha_4 = \frac{\gamma}{\chi} - 1, \\ \alpha_5 = \frac{\Delta t}{2} \left(\frac{\gamma}{\chi} - 2 \right), \quad \alpha_6 = \Delta t(1 - \gamma), \quad \alpha_7 = \Delta t\gamma, \end{aligned} \tag{109}$$

in which $\gamma = 0.5$ and $\chi = 0.25$. Based on the iteration method, Eq. (106) is solved at any time step and modified velocity and acceleration vectors are calculated as follows:

$$\ddot{d}_{i+1} = \alpha_0(d_{i+1} - d_i) - \alpha_2 \dot{d}_i - \alpha_3 \ddot{d}_i, \tag{110}$$

$$\dot{d}_{i+1} = \dot{d}_i + \alpha_6 \ddot{d}_i + \alpha_7 \ddot{d}_{i+1}. \tag{111}$$

Then for the next time step, the modified velocity and acceleration vectors in Eqs. (110) and (111) are employed and all these procedures mentioned above are repeated.

9 Numerical results

In this section, the dynamic response of the present structure is studied for different parameters. For this purpose, a sandwich plate with length to width ratio of $a/b = 1$, length to total thickness of $a/h = 10$, length of the vertical cell rib to length of the inclined cell rib of $d/l = 1$, thickness to length of the inclined cell rib of $t/l = 0.0138$ and inclined angle of rosmarinic acid is considered. Furthermore, the explosive weight is $W = 5$ kg and distance of blast center to center of the structure is chosen, $R = 1$ m [44].

9.1 Material properties

The material properties of the core and facesheets are as follows.

9.1.1 Auxetic honeycomb core layer

Young’s modulus of $E = 69.2$ GPa, Poisson’s ratio of $\nu = 0.33$ and mass density of $\rho = 2700$ kg/m³ [33].

9.1.2 Facesheets

The facesheets are made from epoxy reinforced by carbon fibers and CNTs with the following properties [36]:

9.1.2.1 Epoxy Young’s modulus: $E^M = (3.51 - 0.0034T + 0.142H)$ GPa, Poisson’s ratio:

$\nu^M = 0.3$, density: $\rho^M = 1200$ kg/m³, thermal expansion coefficient: $\alpha^M = 45(1 + 0.001\Delta T) \times 10^{-6}$ K⁻¹, and moisture coefficient: $\beta^M = 2.68 \times 10^{-3}$ wt%⁻¹.

9.1.2.2 Carbon fibers Young’s modulus: $E_{11}^F = 233.05$ GPa and $E_{22}^F = 23.1$ GPa, shear modulus: $G_{12}^F = 8.96$ GPa, Poisson’s ratio: $\nu^F = 0.2$, density: $\rho^F = 1750$ kg/m³, thermal expansion coefficient: $\alpha_{11}^F = -0.54 \times 10^{-6}$ K⁻¹ and $\alpha_{22}^F = 10.08 \times 10^{-6}$ K⁻¹, and volume percent: $V^F = 0.6$.

9.1.2.3 CNTs Young’s modulus: $E^{CN} = 640(1 - 0.0005\Delta T)$ GPa, Poisson’s ratio: $\nu^{CN} = 0.27$, density: $\rho^{CN} = 1350$ kg/m³, outer diameter: $d^{CN} = 1.4$ nm, thickness: $t^{CN} = 0.34$ nm, length $l^{CN} = 25 \times 10^{-6}$ m, thermal expansion coefficient: $\alpha^{CN} = 4.5361 \times 10^{-6}$ K⁻¹ and $\alpha^{CN} = 4.6677 \times 10^{-6}$ K⁻¹, respectively, at $T = 300$ K, $T = 500$ K and $T = 700$ K.

9.2 Verification

To validate the results of this work, neglecting the core and top face sheet, CNTs as the reinforcement, structural damping, magnetic field, hygrothermal load and viscoelastic medium, the dynamic response of a plate subjected to blast load is studied. Considering the material properties to be the same as in Ref. [34], the dynamic deflection of the structure is shown in Fig. 3. As can be seen, the present results are in good agreement with Ref [34], which shows the accuracy of the obtained results.

9.3 Convergence of DCM

Figure 4 presents the maximum dynamic deflection of the sandwich structure for different grid points of the DCM.

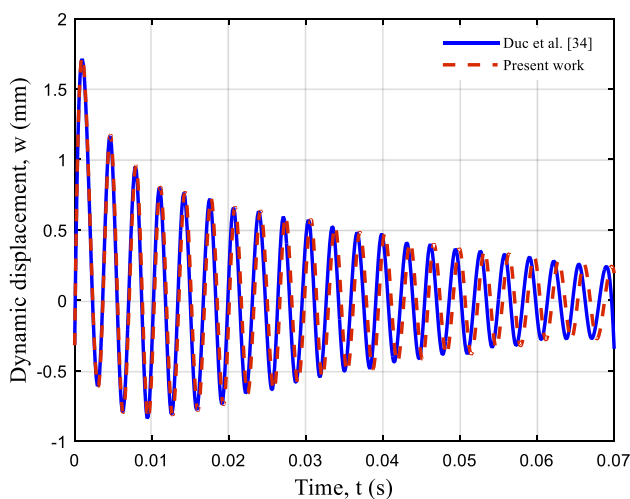


Fig. 3 Validation of present work with Ref. [34]

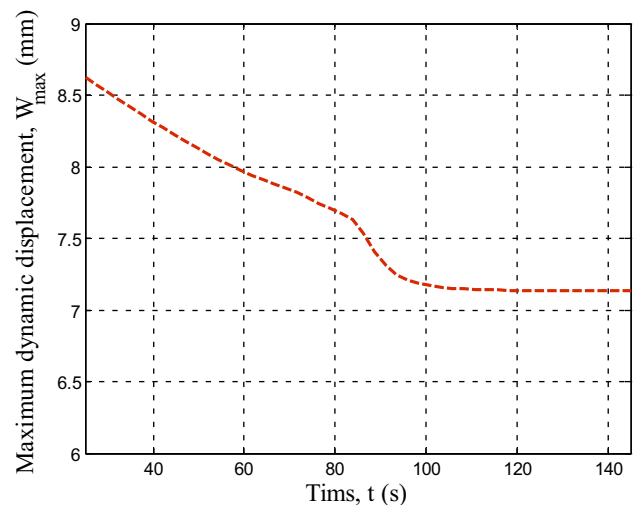


Fig. 4 Convergence and accuracy of DCM

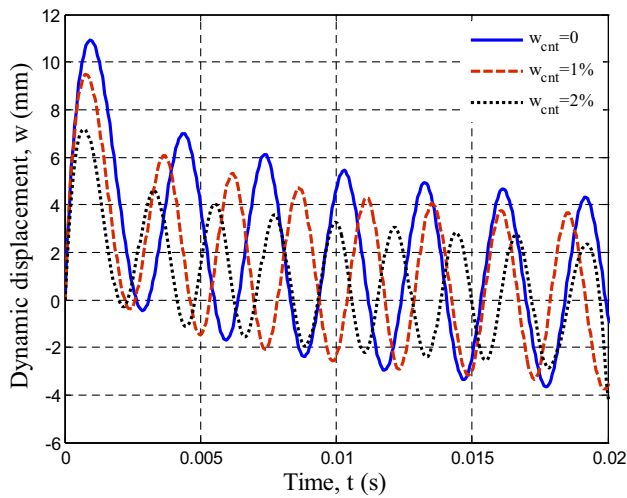


Fig. 5 The effect of CNT weight percent on the dynamic deflection of the structure

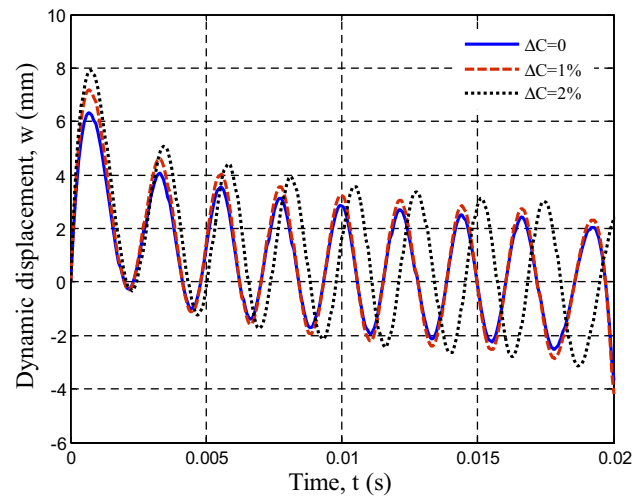


Fig. 7 The effect of the moisture change on the dynamic deflection of the structure

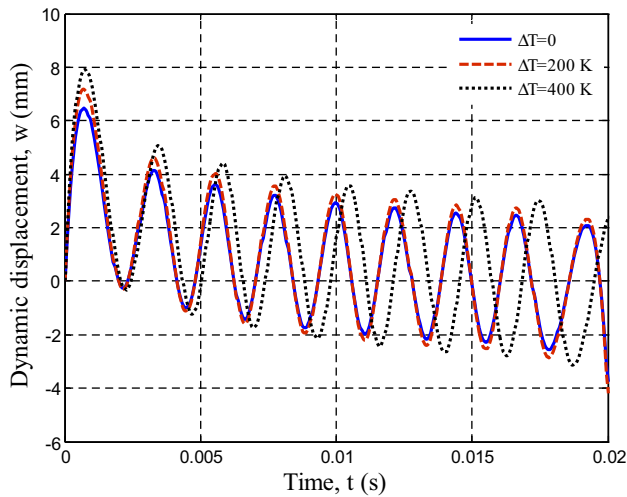


Fig. 6 The effect of the temperature change on the dynamic deflection of the structure

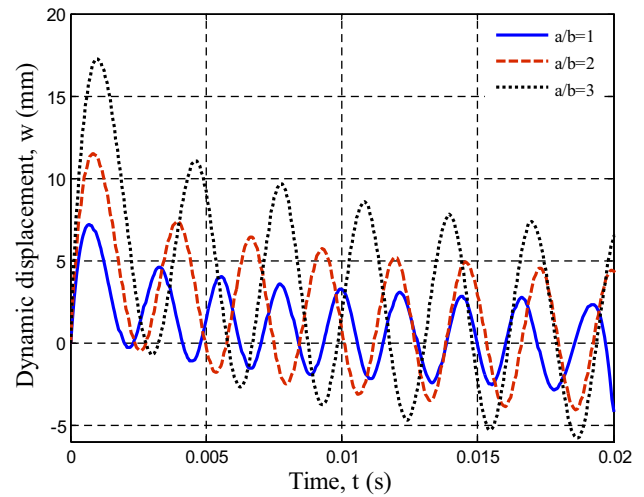


Fig. 8 The effect of the length to width ratio of the sandwich plate on the dynamic deflection of the structure

It can be seen that with increasing the grid points of the DCM, the maximum dynamic deflection decreases rapidly until $N=113$, the changes in the grid points do not affect on the maximum dynamic deflection. However, for accurate results, the grid points in this work are assumed 113.

9.4 The effect of different parameters

The effect of CNT weight percent on the dynamic deflection of the sandwich plates with honeycomb core layer is shown in Fig. 5. As can be seen, reinforcing the facesheets with CNTs leads to stiffer structure and consequently lower dynamic deflection. For example, the maximum dynamic

displacement for $w_{\text{cnt}}=0$ (facesheets without CNTs) is 10.88 while for the facesheets reinforced by 2% CNTs, the maximum dynamic displacement becomes 7.05. It means that by reinforcing the facesheets with 2% CNTs, the maximum dynamic deflection reduces about 54%.

The temperature and moisture change effects on the dynamic displacement of the sandwich plate with respect to the time are illustrated in Figs. 6 and 7. From both the figures, it can be found that with increasing the temperature and moisture changes, the dynamic displacement enhances. This is physically due to this fact that the stiffness of the sandwich structure decreases with increasing the temperature and moisture changes. It is also worth to mention that

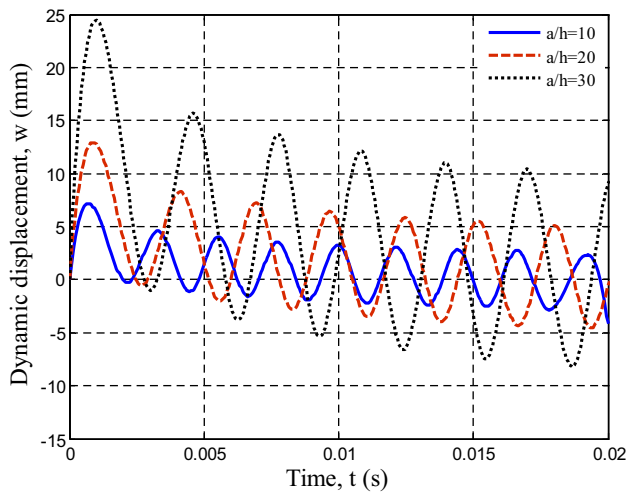


Fig. 9 The effect of the length to total thickness of the sandwich plate on the dynamic deflection of the structure

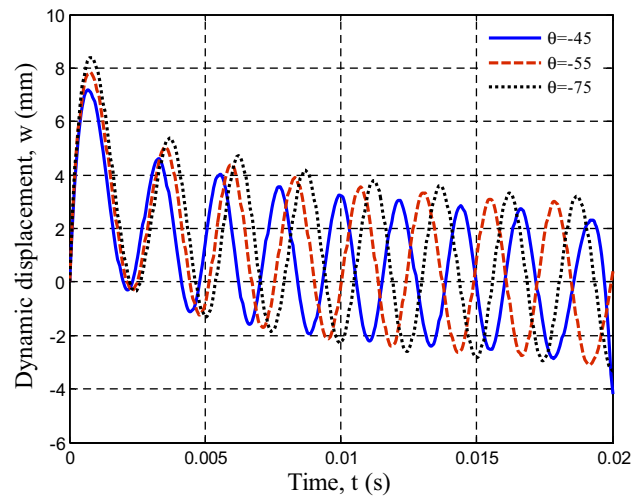


Fig. 11 The effect of the inclined angle of the core cell on the dynamic deflection of the structure

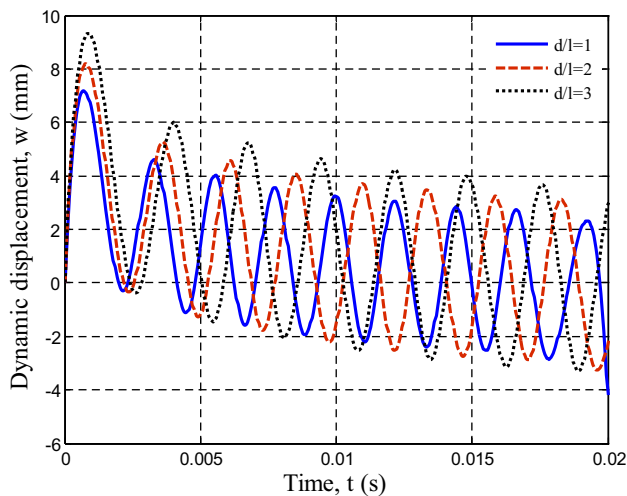


Fig. 10 The effect of the vertical cell rib length to inclined cell rib length on the dynamic deflection of the structure

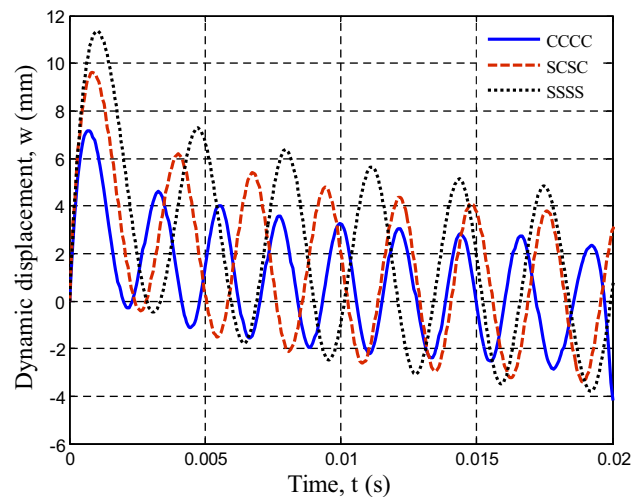


Fig. 12 The effect of the boundary conditions on the dynamic deflection of the structure

the effect of hygrothermal load on the dynamic deflection of the structure is about half time of the effect of CNT weight percent. In other words, considering the hygrothermal environment ($\Delta T = 400 \text{ K}$, $\Delta C = 2\%$), the maximum dynamic deflection decreases about 24%.

The effects of geometrical parameters on the dynamic deflection of the structure are presented in Figs. 8 and 9 for the sandwich plate and in Figs. 10 and 11 for the auxetic honeycomb core cell. Figure 8 shows the effect of length to width ratio of the sandwich plate on the dynamic response. It can be observed that with increasing the length to width ratio, the dynamic deflection increases due to reduction in the stiffness of the sandwich plate. From Fig. 9 which

demonstrates the effect of length to total thickness ratio of the sandwich plate, it can be found that enhancing the length to total thickness ratio leads to higher dynamic displacement. Figures 10 and 11 present the effect of vertical cell rib length to inclined cell rib length (d/l) and inclined angle (θ) on the dynamic response of the structure, respectively. As can be seen, with increasing the d/l and θ , the dynamic deflection increases due to reduction in the stiffness of the core.

For quantitative analysis of the above figures, it can be found that increasing the length to width ratio of the

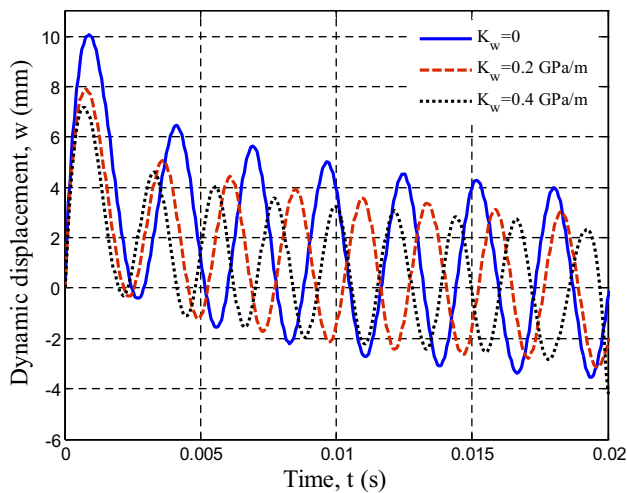


Fig. 13 The effect of the spring constant of viscoelastic medium on the dynamic deflection of the structure

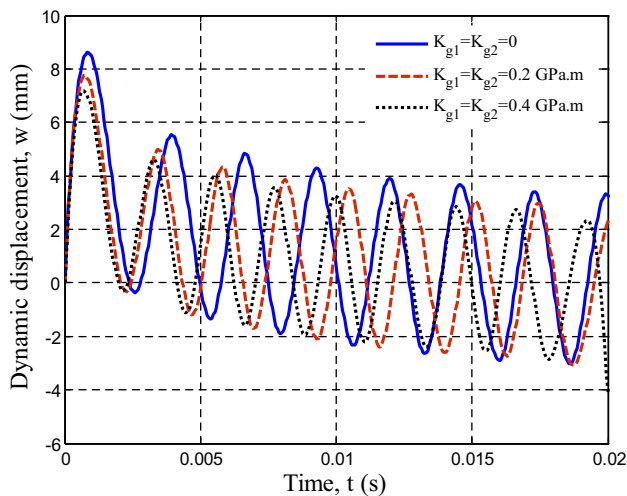


Fig. 14 The effect of the shear constant of viscoelastic medium on the dynamic deflection of the structure

sandwich plate from 1 to 3, the maximum dynamic deflection increases 2.5 times. In addition, with enhancing the length to total thickness ratio of the sandwich plate from 10 to 30, the maximum dynamic deflection becomes 3.5 times greater. For the geometrical parameters of the honeycomb cell, it can be observed that the changes of d/l and inclined angle of core cell increase the maximum dynamic deflection about 34% and 17%, respectively.

Figure 12 depicts the effect of boundary conditions on the dynamic deflection of the sandwich structure. Three types of boundary conditions are considered in this figure. It can be observed that the dynamic deflection of the structure subjected to blast load will be decreased 58% and 34% for the plate with CCCC boundary condition with respect to the

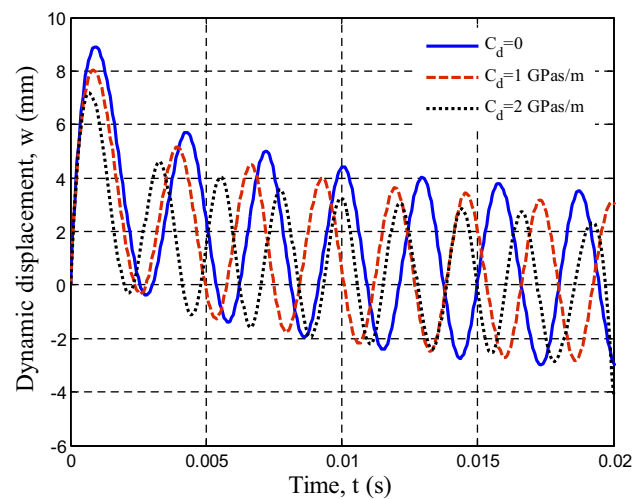


Fig. 15 The effect of the damper constant of viscoelastic medium on the dynamic deflection of the structure

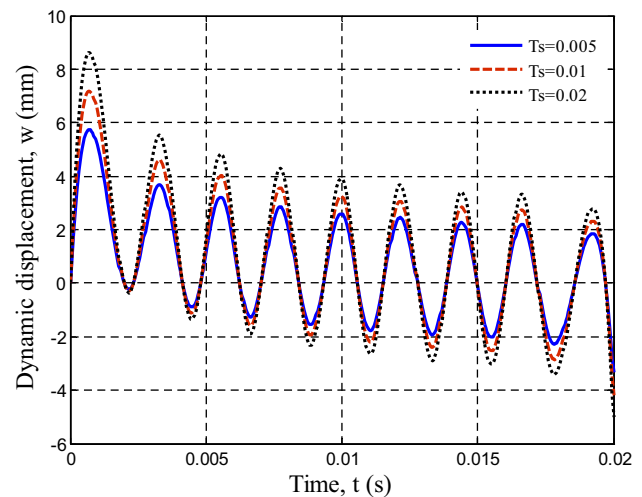


Fig. 16 The effect of the parameter of duration for the blast pulse on the dynamic deflection of the structure

SCSC and SSSS boundary conditions, respectively. It is due to this fact that the sandwich plate with CCCC boundary condition has more bending rigidity with respect to other boundary conditions.

The effect of viscoelastic medium coefficients on the dynamic deflection of the sandwich plate is shown in Figs. 13, 14 and 15, respectively, for spring, shear and damper constants of the foundation. It can be concluded that with increasing the spring, shear and damper constants of the viscoelastic medium, the dynamic deflection decreases. However, it can be found that the existence of viscoelastic medium leads to more strength of the sandwich structure across the blast load.

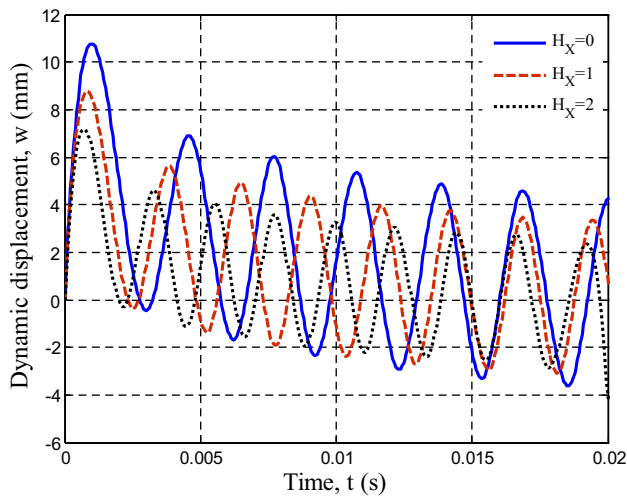


Fig. 17 The effect of the dimensionless magnetic field on the dynamic deflection of the structure

Figure 16 shows the effect of the parameter of duration for the blast pulse (T_s) on the dynamic deflection of the sandwich structure. It can be concluded that with increasing the T_s , the dynamic deflection increases while the phase of the dynamic response does not change.

Figure 17 presents the effect of dimensionless magnetic field ($H_X = \eta H_x^2 / E^c$) on the dynamic response of the sandwich plates. It can be concluded that applying magnetic field to the facesheets decreases the dynamic deflection of the sandwich structure about 42%. It is physically due to this fact that applying magnetic field to the facesheets improves the stiffness of the structure. This considerable effect shows that the magnetic field can be used as an effective controlling parameter for the reduction of the dynamic deflection in sandwich plates under blast load.

Figure 18 is plotted to show the effect of dimensionless structural damping ($G = (g\sqrt{E^c/\rho^c})/a$) on the dynamic deflection of the sandwich structure. As can be observed, considering the structural damping decreases the dynamic deflection due to increase in the energy absorbing. In other words, considering $G=0.2$ decreases the maximum dynamic deflection about 34%. However, it can be concluded that for realistic modeling of the present structure, considering structural damping is essential.

10 Conclusions

Dynamic response of sandwich plates resting on orthotropic viscoelastic medium subjected to blast load was presented in this article. Considering auxetic honeycomb core, multiphase nanocomposite facesheets, structural damping, hygrothermal environment, 2D magnetic field, RZT and

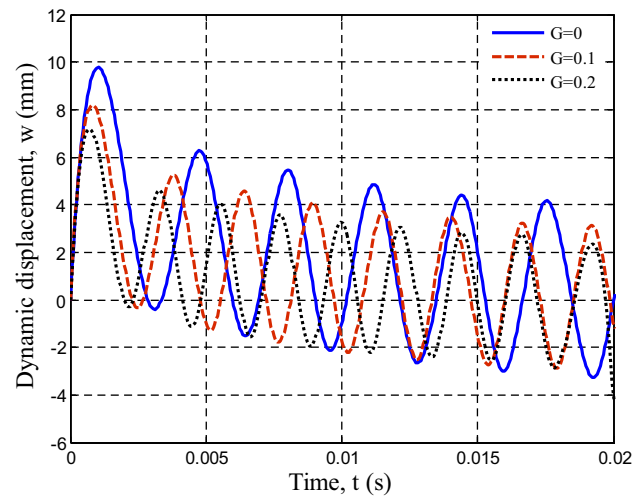


Fig. 18 The effect of the structural damping on the dynamic deflection of the structure

novel numerical method of DC were the main contributions of this work. The Halpin–Tsai and Kelvin–Voigt theories were used for calculating the effective material properties of facesheets and considering viscoelastic property of the structure, respectively. The motion equations were derived by RZT, energy method and Hamilton’s principle. Based on DC and Newmark methods, the dynamic deflection of the sandwich structure was obtained so that the effects of various parameters such as blast load, viscoelastic foundation, structural damping, magnetic field, volume fraction of CNTs, temperature and moisture changes, geometrical parameters of honeycomb layer and sandwich plate were shown. The most findings of this work were:

- By reinforcing the facesheets with 2% CNTs, the maximum dynamic deflection reduces about 54%.
- Considering the hygrothermal environment ($\Delta T = 400$ K, $\Delta C = 2\%$), the maximum dynamic deflection decreases about 24%.
- With enhancing the length to total thickness ratio of the sandwich plate from 10 to 30, the maximum dynamic deflection becomes 3.5 times greater.
- The changes of d/l and inclined angle of core cell increase the maximum dynamic deflection about 34% and 17%, respectively.
- The dynamic deflection of the structure subjected to blast load will be decreased 58% and 34% for the plate with CCCC boundary condition with respect to the SCSC and SSSS boundary conditions, respectively.
- It can be concluded that with increasing the parameter of duration for the blast pulse, the dynamic deflection increases while the phase of the dynamic response does not change.

- The magnetic field can be used as an effective controlling parameter for the reduction of the dynamic deflection in CNT-reinforced sandwich plates under blast load.
- As can be observed, considering the structural damping decreases the dynamic deflection due to increase in the energy absorbing.

References

1. Wilkins DJ, Bert CW, Egle DM (1970) Free vibrations of orthotropic sandwich conical shells with various boundary conditions. *J Sound Vib* 13:211–228
2. Allam MNM, Zenkour AM, El-Mekawy HF (2010) Bending response of inhomogeneous fiber-reinforced viscoelastic sandwich plates. *Acta Mech* 209:231–248
3. Mahapatra TR, Kar VR, Panda SK (2016) Large amplitude vibration analysis of laminated composite spherical panels under hygrothermal environment. *Int J Struct Stab Dyn* 16:1450105
4. Nguyen LB, Thai CH, Nguyen-Xua H (2016) A generalized unconstrained theory and isogeometric finite element analysis based on Bézier extraction for laminated composite plates. *Eng Comput* 32:457–475
5. Mahapatra TR, Panda SK (2016) Nonlinear free vibration analysis of laminated composite spherical shell panel under elevated hygrothermal environment: a micromechanical approach. *Aerosp Sci Technol* 49:276–288
6. Mahapatra TR, Panda SK, Kar VR (2016) Nonlinear flexural analysis of laminated composite panel under hygro-thermo-mechanical loading—a micromechanical approach. *Int J Comput Meth* 13:1650015
7. Mahapatra TR, Panda SK, Kar VR (2016) Nonlinear hygro-thermo-elastic vibration analysis of doubly curved composite shell panel using finite element micromechanical model. *Mech Adv Mater Struct* 23:1343–1359
8. Mahapatra TR, Panda SK, Kar VR (2016) Geometrically nonlinear flexural analysis of hygro-thermo-elastic laminated composite doubly curved shell panel. *Int J Mech Mat Des* 12:153–171
9. Kolahchi R, Keshtegar B, Fakhari MH (2017) Optimization of dynamic buckling for sandwich nanocomposite plates with sensor and actuator layer based on sinusoidal visco-piezoelectricity theories using Grey Wolf algorithm. *J Sandw Struct Mat*. <https://doi.org/10.1177/1099636217731071>
10. Duc ND, Quan TQ, Khoa N (2017) New approach to investigate nonlinear dynamic response and vibration of imperfect functionally graded carbon nanotube reinforced composite double curved shallow shells subjected to blast load and temperature. *Aerosp Sci Technol*. <https://doi.org/10.1016/j.ast.2017.09.031>
11. Duc ND, Jaechong Lee T, Nguyen-Thoi T, Thang PT (2017) Static response and free vibration of functionally graded carbon nanotube-reinforced composite rectangular plates resting on Winkler–Pasternak elastic foundations. *Aerosp Sci Technol* 68:391–402
12. Thanh NV, Khoa ND, Tuan ND, Phuong T, Duc ND (2017) Nonlinear dynamic response and vibration of functionally graded carbon nanotubes reinforced composite (FG-CNTRC) shear deformable plates with temperature dependence material properties and surrounded on elastic foundations. *J Therm Stress* 40(10):1254–1274
13. Duc ND, Cong PH, Tuan ND, Phuong T, Thanh NV (2017) Thermal and mechanical stability of functionally graded carbon nanotubes (FG CNT)-reinforced composite truncated conical shells surrounded by the elastic foundations. *Thin Wall Struct* 115:300–310
14. Mahapatra TR, Mehar K (2017) Nonlinear thermoelastic deflection of temperature-dependent FGM curved shallow shell under nonlinear thermal loading. *J Therm Stress* 40:1184–1199
15. Kar VR, Mahapatra TR, Panda SK (2017) Effect of different temperature load on thermal postbuckling behaviour of functionally graded shallow curved shell panels. *Compos Struct* 160:236–247
16. Katariya PV, Panda SK, Mahapatra TR (2017) Prediction of nonlinear eigenfrequency of laminated curved sandwich structure using higher-order equivalent single-layer theory. *J Sandw Struct Mat*. <https://doi.org/10.1177/1099636217728420>
17. Mehar K, Panda SK, Mahapatra TR (2017) Theoretical and experimental investigation of vibration characteristic of carbon nanotube reinforced polymer composite structure. *Int J Mech Sci* 133:319–329
18. Mehar K, Panda SK, Mahapatra TR (2017) Thermoelastic nonlinear frequency analysis of CNT reinforced functionally graded sandwich structure. *Eur J Mech A Solids* 65:384–396
19. Mehar K, Panda SK (2017) Thermal free vibration behavior of FG-CNT reinforced sandwich curved panel using finite element method. *Polym Compos* 39:2751–2764
20. Kolahchi R, Zarei MSh, Hajmohammad MH, Nouri A (2017) Wave propagation of embedded viscoelastic FG-CNT-reinforced sandwich plates integrated with sensor and actuator based on refined Zigzag theory. *Int J Mech Sci* 130:534–545
21. Zarei MSh, Azizkhani MB, Hajmohammad MH, Kolahchi R (2017) Dynamic buckling of polymer-CNT-fiber multiphase nanocomposite viscoelastic laminated conical shells in hygrothermal environments. *J Sandw Struct Mat*. <https://doi.org/10.1177/1099636217743288>
22. Hajmohammad MH, Zarei MSh, Nouri A, Kolahchi R (2017) Dynamic buckling of sensor/functionally graded-carbon nanotubes reinforced laminated plates/actuator based on sinusoidal-visco piezoelectricity theories. *J Sandw Struct Mater*. <https://doi.org/10.1177/1099636217720373>
23. Katariya PV, Hirwani ChK, Panda SK (2018) Geometrically nonlinear deflection and stress analysis of skew sandwich shell panel using higher-order theory. *Eng Comput*. <https://doi.org/10.1007/s00366-018-0609-3>
24. Hirwani ChK, Panda SK, Mahapatra TR (2018) Nonlinear finite element analysis of transient behavior of delaminated composite plate. *J Vib Acous* 140:021001
25. Sharma N, Mahapatra TR, Panda SK (2018) Numerical analysis of acoustic radiation responses of shear deformable laminated composite shell panel in hygrothermal environment. *J Sound Vib* 431:346–366
26. Qin Q, Yuan Ch, Zhang J, Wang TJ (2014) Large deflection response of rectangular metal sandwich plates subjected to blast loading. *Eur J Mech A Solids* 47:14–22
27. Hou X, Deng Z, Zhang K (2016) Dynamic crushing strength analysis of auxetic honeycombs. *Acta Mech Solida Sin* 29:490–501
28. Hirwani ChK, Panda SK, Mahapatra TR, Mandal SK, De AK (2017) Dynamic behaviour of delaminated composite plate under blast loading. In: ASME 2017 gas turbine India conference, India, p V002T05A032. <https://doi.org/10.1115/GTINDIA2017-4847>
29. Ling Q, He Y, He Y, Pang Ch (2017) Dynamic response of multi-body structure subjected to blast loading. *Eur J Mech A Solids* 64:46–57
30. Duc ND, Seung-Eock K, Cong PH, Anh NT, Khoa ND (2017) Dynamic response and vibration of composite double curved shallow shells with negative Poisson's ratio in auxetic honeycombs core layer on elastic foundations subjected to blast and damping loads. *Int J Mech Sci* 133:504–512
31. Duc ND, Seung-Eock K, Tuan ND, Tran P, Khoa ND (2017) New approach to study nonlinear dynamic response and vibration of

- sandwich composite cylindrical panels with auxetic honeycomb core layer. *Aerosp Sci Technol* 70:396–404
32. Duc ND, Quan TQ, Khoa ND (2017) New approach to investigate nonlinear dynamic response and vibration of imperfect functionally graded carbon nanotube reinforced composite double curved shallow shells subjected to blast load and temperature. *Aerosp Sci Technol* 71:360–372
 33. Duc ND, Cong PH (2017) Nonlinear dynamic response and vibration of sandwich composite plates with negative Poisson's ratio in auxetic honeycombs. *J Sandw Struct Mater*. <https://doi.org/10.1177/1099636216674729>
 34. Duc ND, Tuan ND, Phuong T, Quan TQ (2017) Nonlinear dynamic response and vibration of imperfect shear deformable functionally graded plates subjected to blast and thermal loads. *Mech Adv Mater Struct* 24(4):318–329
 35. Tessler A, Sciuva MD, Gherlone M (2010) A consistent refinement of first-order shear deformation theory for laminated composite and sandwich plates using improved zigzag kinematics. *J Mech Mat Struct* 5:341–362
 36. Ebrahimi F, Habibi S (2018) Nonlinear eccentric low-velocity impact response of polymer-CNT-fiber multi scale nanocomposite plate resting on elastic foundations in hygrothermal environments. *Mech Adv Mater Struct* 25:425–438
 37. Chetan SJ (2012) *Micromechanics and modelling of adaptive shape memory composites*. LAMBERT Academic Publishing, England
 38. Manmohan DG, Vasant A, Matsagar A, Gupta K (2011) Dynamic responses of stiffened plates under air blast. *Int J Protect Struct* 2:139–155
 39. Kadid A (2011) Stiffened plates subjected to uniform loading. *J Civil Eng Manag* 14:155–161
 40. Vasilis K, Solomos G (2013) Calculation of blast loads for application to structural components. Publications Office of the European Union, EUR Scientific and Technical Research series, Luxembourg
 41. Lakes R (2009) *Viscoelastic materials*. Cambridge University Press, New York
 42. Kolahchi R, Hosseini H, Esmailpour M (2016) Differential cubature and quadrature-Bolotin methods for dynamic stability of embedded piezoelectric nanoplates based on visco-nonlocal-piezoelectricity theories. *Compos Struct* 157:174–186
 43. Simsek M (2010) Non-linear vibration analysis of a functionally graded Timoshenko beam under action of a moving harmonic load. *Compos Struct* 92:2532–2546
 44. Mohammadzadeh B, Noh HCh (2017) Analytical method to investigate nonlinear dynamic responses of sandwich plates with FGM faces resting on elastic foundation considering blast loads. *Compos Struct* 174:142–157
- Publisher's Note** Springer Nature remains neutral with regard to jurisdictional claims in published maps and institutional affiliations.